Commun Nonlinear Sci Numer Simulat 70 (2019) 257–270

Contents lists available at ScienceDirect

Commun Nonlinear Sci Numer Simulat

journal homepage: www.elsevier.com/locate/cnsns

Short Communication

On power law scaling dynamics for time-fractional phase field models during coarsening

Jia Zhao[a], Lizhen Chen[b,*], Hong Wang[c]

[a] Utah State University, Logan, UT, USA
[b] Beijing Computational Science Research Center,Beijing, China
[c] University of South Carolina, Columbia, SC,USA

ARTICLE INFO

Article history:
Received 14 March 2018
Revised 15 October 2018
Accepted 15 October 2018
Available online 24 October 2018

ABSTRACT

In this paper, the energy scaling behavior of the time-fractional phase field models is investigated. We report a seminal observation that the effective free energy of the time-fractional phase field models obeys a general power-law scaling dynamics during coarsening. Mainly, the effective free energy and roughness in the time-fractional phase field models scale by following a similar power law as the integer phase field models, where the power is linearly proportional to the fractional order. This general scaling law is verified numerically against several classes of phase field models, including the Cahn–Hilliard equation with different types of variable mobilities and the molecular beam epitaxy models. This new finding opens potential paths of applying time-fractional phase field models in studying anomalous coarsening dynamics.

1. Introduction

Phase field models have been widely exploited to study material, physical and biology systems [17,33,36,45,45,50,53]. One important application of phase field models is to study coarsening dynamics [11,13,20,22,52], which is a widely observed phenomenon in material systems involving micro-structures. It is characterized by the dissipation of excessive Helmholtz free energy and the growth of a characteristic length scale [11]. Mainly if we introduce a characteristic length scale $R(t)$, it grows like a power function in time, i.e., $R(t) \sim O(t^{\frac{1}{\alpha}})$, where $\alpha > 0$ indicates the growth order. In other words, $R(t)^{\alpha} - R(t_0)^{\alpha} \approx c(t - t_0)$ for some positive constant c. Or one could characterize the coarsening by an effective energy $E(t)$, which decays like a power function in time, i.e. $E(t) \sim O(t^{-\frac{1}{\beta}})$, where $\beta > 0$ indicates the order. In other words, $E(t)^{\beta} - E(t_0)^{\beta} \approx c(t_0 - t)$ with c some positive constant. This is known as a power law scaling dynamics, which has already been widely investigated both theoretically and numerically [11,19,20]. For instance the Cahn–Hilliard equation with smooth double-well potential and phase-dependent diffusion mobility is studied in [11], where the authors show that the coarsening dynamics of the Cahn–Hilliard equation is relative to the mobility coefficient: for CH equation with constant mobility, the free energy scales as $O(t^{-\frac{1}{3}})$; for the two-sided degenerate mobility, the free energy scales as $O(t^{-\frac{1}{4}})$, which is independent of the volume fraction of each phase [11]; for the one-sided degenerate mobility, the free energy scales depending on the volume fraction of the phases. The coarsening of the molecular beam epitaxy (MBE) model has also been investigated [43]: for

* Corresponding author.
E-mail addresses: jia.zhao@usu.edu (J. Zhao), lzchen@csrc.ac.cn (L. Chen), hwang@mailbox.sc.edu (H. Wang).

https://doi.org/10.1016/j.cnsns.2018.10.019
1007-5704/

the MBE model with slope selection, the free energy scales as $O(t^{-\frac{1}{3}})$ and the roughness growth scales as $O(t^{\frac{1}{3}})$; for the MBE model without slope selection, the roughness growth scales as $O(t^{\frac{1}{2}})$. However, all these studies focus on mixtures without long-range interactions. For the more complex material mixture, taking liquid crystal polymer solution as an example or some materials with elastic memory, the scaling dynamics would change dramatically [29,40,41]. To study such kinds of anomalous coarsening dynamics with a simplified reaction-diffusion PDE (without considering the hydrodynamics), a new mechanism with nonlinear evolution property should be added.

One straightforward starting point to study such anomalous coarsening dynamics would be utilizing the fractional derivatives, i.e., formulating fractional phase field models. Fractional phase field models have been studied in the last few years and have quickly attracted increased attention ever since. The study of fractional phase-field models is motivated by the significantly increased applications of fractional partial differential equations (FPDEs) to a wide variety of areas [30,31,34] and the rapid developed mathematical, numerical and computational analysis of FPDEs over the past few decades. The concept of FPDEs can be explained in the context of anomalously diffusive transport. The classical second-order diffusion PDE was first presented by Fick in his study on how water and nutrients travel through cell membranes. Einstein and Pearson derived the diffusion PDE independently from first principles and random walk under the common assumptions of (i) the existence of a mean free path and (ii) the existence of a mean time taken to perform a jump in the particle movements in the underlying processes. Under these assumptions, the variance of a particle excursion distance is finite. The central limit theorem concludes that the probability of finding a particle somewhere in space satisfies a Gaussian distribution, which gives a probabilistic description of the Fickian diffusion. In the last few decades more and more diffusion processes were found to be non-Fickian, ranging from the signaling of biological cells [32], anomalous electrodiffusion in nerve cells [21], foraging behavior of animals [35] to viscoelastic and visco-plastic flow [34] and solute transport in groundwater [5]. In these cases either the particle movements have many long jumps or have experienced long waiting times, namely, the assumptions (i) or (ii) is violated. Consequently, the processes can have large deviations from the stochastic process of Brownian motion, leading to anomalously diffusive transport that exhibits heavy tails either in space or in time. Consequently, classical integer-order PDE models fail to provide an accurate description of these problems. In contrast, it has been shown that these anomalously diffusive transport can be better modeled by space-fractional PDE (for super-diffusive transport) or time-fractional PDE (for sub-diffusive transport) [30,31].

The same principle applies to phase-field models. If the coarsening dynamic processes experience some long-range spatial interaction and so the assumption (i) is violated, the corresponding phase-field models may be better described by space-fractional phase-field models [39]. As a matter of fact, the original phase-field model was expressed in terms of an integration of Helmholtz free energy that has a nonlocal spatial interaction [8]. It was approximated by a Laplacian operator just for the modeling, mathematical and numerical simplicity. On the other hand, when the material during the coarsening process exhibits the memory effect, the assumption (ii) is violated. The corresponding phase-field model may be described by a time-fractional phase-field model [27].

In this paper, we study time-fractional phase-field models. Our major contribution is presenting a seminal observation that time fractional phase field models have a general power laws scaling property. *The scaling of effective free energy/roughness in the time-fractional phase field models during coarsening follows a similar power law as the integer phase field models, where the power is linearly proportional to the fractional order* α. By far, this is the first report in the literature. Several numerical examples of fractional phase field models with specific choices of free energies and mobilities are presented to verify this new observation. The rigorous asymptotic analysis of this interesting correlation will be pursed in our future work.

In the rest of this paper, we will introduce the classical and fractional phase field models in Section 2. And in Section 3, we will provide the numerical approximations for the fractional phase field models. Afterward, we will present the power scaling laws for the effective free energy and roughness of the time-fractional phase field models in Section 4. In the end, we draw a brief conclusion and point out possible future research directions.

2. Phase field models

In this section, we first briefly introduce the classical (integer) phase field models and introduce the corresponding time-fractional phase field models subsequently. For the detailed derivation and properties of phase field models, readers are referred to [9,34,39] and the references therein.

2.1. Classical phase field models

Consider a bounded domain Ω with smooth boundary $\partial\Omega$. The inner product on Ω is denoted as $(f,g)=\int_\Omega fg d\mathbf{x}$, for all $f, g\in L^2(\Omega)$. The L^2 norm of f, for all $f\in L^2(\Omega)$ is denoted as $\|f\|=\sqrt{(f,f)}$.

We focus on a material system with two components. Introduce a phase variable ϕ to represent the volume fraction of one component, such that $1-\phi$ represents the volume fraction of the other component. For the situations of a material system with multiple components, more phase variables should be introduced. We also introduce the notation E to represent the total free energy. Given the explicit expression of E, there are usually two types of phase field equations, namely the

Allen–Cahn type (AC) equation, and the Cahn–Hilliard type (CH) equation [2,7,8]. Both equations are in the categories of gradient flow models.

For the Allen–Cahn equation, the rate of change $\partial_t\phi$ is in the direction of decreasing gradient of the free energy functional $E(\phi)$, which reads as

$$\begin{cases} \partial_t\phi = -\lambda\frac{\delta E}{\delta\phi}, \text{ in } \Omega_T = \Omega\times(0,T], \\ \nabla\phi\cdot\mathbf{n} = 0, \text{ on } \partial\Omega\times(0,T], \\ \phi = \phi_0, \text{ in } \Omega_0 = \Omega\times\{0\}, \end{cases} \tag{2.1}$$

where λ is the mobility parameter, and $\frac{\delta E}{\delta\phi}$ is the chemical potential (the functional derivative of E with respect to ϕ). Its energy dissipation law is

$$\frac{dE}{dt} = \int_\Omega \frac{\delta E}{\delta\phi}\frac{\delta\phi}{\delta t}d\mathbf{x} = \int_\Omega -\lambda\Big(\frac{\delta E}{\delta\phi}\Big)^2 d\mathbf{x} \le 0. \tag{2.2}$$

One other property of Allen–Cahn equation is its lacking of mass conservation, i.e.

$$\frac{d}{dt}\int_\Omega \phi d\mathbf{x} = \int_\Omega -\lambda\frac{\delta E}{\delta\phi}d\mathbf{x} \neq 0. \tag{2.3}$$

The Cahn–Hilliard equation could be interpreted as derived by following the Fick's first law, where the flux flows from regions of high chemical potential to low chemical potential regions, which reads as

$$\begin{cases} \partial_t\phi = \nabla\cdot(\lambda\nabla\frac{\delta E}{\delta\phi}), \text{ in } \Omega_T = \Omega\times(0,T], \\ \nabla\phi\cdot\mathbf{n} = 0, \nabla\frac{\delta E}{\delta\phi}\cdot\mathbf{n} = 0, \text{ on } \partial\Omega\times(0,T], \\ \phi = \phi_0, \text{ in } \Omega_0 = \Omega\times\{0\}, \end{cases} \tag{2.4}$$

where λ is the motility parameter. For the Cahn–Hilliard equation, it possesses an energy dissipation law as follows

$$\frac{dE}{dt} = \int_\Omega \frac{\delta E}{\delta\phi}\frac{\delta\phi}{\delta t}d\mathbf{x} = -\int_\Omega \lambda|\nabla\frac{\delta E}{\delta\phi}|^2 d\mathbf{x} + \int_{\partial\Omega}\lambda\frac{\delta E}{\delta\phi}\nabla\frac{\delta E}{\delta\phi}\cdot\mathbf{n}dS \le 0, \tag{2.5}$$

and a mass conservation property as

$$\frac{d}{dt}\int_\Omega \phi d\mathbf{x} = \int_\Omega \nabla\cdot(\lambda\nabla\frac{\delta E}{\delta\phi})d\mathbf{x} = \int_{\partial\Omega}\lambda\nabla\frac{\delta E}{\delta\phi}\cdot\mathbf{n}ds = 0. \tag{2.6}$$

The major difference of these two models is the total volume of phase variable ϕ is conserved in the Cahn–Hilliard equation, whereas it is not in the Allen–Cahn equation. Due to such difference, the Cahn–Hilliard equation is usually used to study multiphase fluid flows, spinodal decomposition (coarsening), nucleation etc [3,6,8,11,48,49], where the total volume of the phase ϕ is conserved. On the other hand, the Allen–Cahn equation is usually used to study crystal growth, solid-liquid phase transition etc [23,26,47,51], where the total volume of the phase ϕ is not conserved. Nevertheless, both the Allen–Cahn equation and the Cahn–Hilliard equation are thermodynamically consistent, i.e. their total free energy is none increasing in time (at constant temperature).

2.2. Time fractional phase field models

Next, we introduce the corresponding time-fractional phase field models, i.e., the time-fractional Allen–Cahn (FAC) type equations and the time-fractional Cahn–Hilliard (FCH) type equations. Unlike the integer phase field models which could be derived from energy variation, there is not a clear physical or thermodynamical guidance available for deriving the fractional phase field models yet. One widely used approach is simply replacing the integer time derivatives by the fractional time derivatives.

Denote the Caputo fractional derivative of order α as ${}_0^C D_t^\alpha$ (with $\alpha\in(0,1]$), which is defined by Li and Xu [25,34]

$${}_0^C D_t^\alpha\phi(x,t) := \begin{cases} \frac{1}{\Gamma(1-\alpha)}\int_0^t \frac{\partial\phi(x,\tau)}{\partial\tau}\frac{d\tau}{(t-\tau)^\alpha}, & 0<\alpha<1, \\ \frac{\partial\phi}{\partial t}, & \alpha = 1, \end{cases} \tag{2.7}$$

with $\Gamma(\cdot)$ the Gamma function. The Caputo type time-fractional differential operator provides a mean to model the sub-diffusive or long time memory behavior. For simplicity, we consider periodic boundary conditions for the FPDEs in this paper. Thus, the time-fractional Allen–Cahn equation reads

$$\begin{cases} {}_0^C D_t^\alpha\phi = -\lambda\frac{\delta E}{\delta\phi}, \text{ in } \Omega_T = \Omega\times(0,T], \\ \phi = \phi_0, \text{ in } \Omega_0 = \Omega\times\{0\}. \end{cases} \tag{2.8}$$

and the time-fractional Cahn–Hilliard equation reads

$$\begin{cases} {}_0^C D_t^\alpha\phi = \nabla\cdot(\lambda\nabla\frac{\delta E}{\delta\phi}), \text{ in } \Omega_T = \Omega\times(0,T], \\ \phi = \phi_0, \text{ in } \Omega_0 = \Omega\times\{0\}. \end{cases} \tag{2.9}$$

With this ad-hoc formulation of fractional phase field models, there are no theoretical results on elucidating the intrinsically thermodynamic laws in them. But all available numerical study do verify their obeying similar energy dissipation laws as their corresponding integer phase field models [9,27,39].

3. Numerical approximation of the time fractional phase field models

In order to numerically study the time-fractional phase field models, some efficient and stable numerical approximations are necessary. Since numerical analysis is not the major focus of this paper, we briefly introduce our numerical strategies. Readers are encouraged to read [9,38] and the references therein for details.

3.1. Stabilized fast time discretization

Overall, there are mainly two major difficulties in discretizing the models in time: the time-fractional operator, and the nonlinear terms. Here we provide general numerical techniques to deal with these issues as follows.

Consider the time domain $[0\ T]$, which are discretized at $\{t_i\}_{i=1}^N$ such that $0 = t_0 < t_1 < t_2 \cdots < t_N = T$. For the time fractional operator, we utilize the fast evaluation strategy proposed in [16,46]. Recall the Caputo fractional derivative of order α $(0 < \alpha < 1)$ [1,28]

$$ {}_0^C D_t^\alpha \phi(x,t) = \frac{1}{\Gamma(1-\alpha)} \int_0^t \frac{\partial \phi(x,\tau)}{\partial \tau} \frac{d\tau}{(t-\tau)^\alpha}. \tag{3.1} $$

The fractional-in-time derivative term is split into a sum of local part and history part as following:

$$ \begin{aligned} {}_0^C D_t^\alpha \phi(\mathbf{x}, t_{k+1}) &= \frac{1}{\Gamma(1-\alpha)} \int_0^{t_{k+1}} \frac{\phi_s(\mathbf{x},s)}{(t-s)^\alpha} ds, \\ &= \frac{1}{\Gamma(1-\alpha)} \int_{t_k}^{t_{k+1}} \frac{\phi_s(\mathbf{x},s)}{(t-s)^\alpha} ds + \frac{1}{\Gamma(1-\alpha)} \int_0^{t_k} \frac{\phi_s(\mathbf{x},s)}{(t-s)^\alpha} ds \\ &:= C_l(t_{k+1}) + C_h(t_{k+1}), \end{aligned} \tag{3.2} $$

which are approximated respectively as follows:

$$ C_l(t_{k+1}) \approx \frac{\phi(\mathbf{x}, t_{k+1}) - \phi(\mathbf{x}, t_k)}{\Delta t_{k+1}^\alpha \Gamma(2-\alpha)}, \tag{3.3} $$

and

$$ \begin{aligned} C_h(t_{k+1}) &= \frac{1}{\Gamma(1-\alpha)} \left[\frac{\phi(\mathbf{x}, t_k)}{\Delta t_{k+1}^\alpha} - \frac{\phi(\mathbf{x}, t_0)}{t_{k+1}^\alpha} - \alpha \int_0^{t_k} \frac{\phi(\mathbf{x},s)}{(t-s)^{1+\alpha}} ds \right] \\ &\approx \frac{1}{\Gamma(1-\alpha)} \left[\frac{\phi(\mathbf{x}, t_k)}{\Delta t_{k+1}^\alpha} - \frac{\phi(\mathbf{x}, t_0)}{t_{k+1}^\alpha} - \alpha \sum_{i=1}^{K_{exp}} \omega_i \int_0^{t_k} e^{-(t_{k+1}-\tau)s_i} \phi(\mathbf{x},\tau) d\tau \right] \\ &= \frac{1}{\Gamma(1-\alpha)} \left[\frac{\phi(\mathbf{x}, t_k)}{\Delta t_{k+1}^\alpha} - \frac{\phi(\mathbf{x}, t_0)}{t_{k+1}^\alpha} - \alpha \sum_{i=1}^{K_{exp}} \omega_i U_{hist,i}(t_{k+1}) \right], \end{aligned} \tag{3.4} $$

with

$$ \begin{aligned} U_{hist,i}(t_{k+1}) &= \int_0^{t_k} e^{-(t_{k+1}-\tau)s_i} \phi(\mathbf{x},\tau) d\tau \\ &= e^{-s_i \Delta t_{k+1}} U_{hist,i}(t_k) + \int_{t_{k-1}}^{t_k} e^{-(t_{k+1}-\tau)s_i} \phi(\mathbf{x},\tau) d\tau \\ &\approx e^{-s_i \Delta t_{k+1}} U_{hist,i}(t_k) + \frac{e^{-s_i \Delta t_{k+1}}}{s_i^2 \Delta t_k} \Big[(e^{-s_i \Delta t_k} - 1 + s_i \Delta t_k) \phi(\mathbf{x}, t_k) \\ &\quad + (1 - e^{-s_i \Delta t_k} - e^{-s_i \Delta t_k} s_i \Delta t_k) \phi(\mathbf{x}, t_{k-1}) \Big]. \end{aligned} $$

Therefore, the fast evaluation of the Caputo fractional derivative is summarized as

$$ {}_0^C D_t^\alpha \phi^{n+1} = \frac{\phi^{n+1} - \phi^n}{\Delta t_{n+1}^\alpha \Gamma(2-\alpha)} + \frac{1}{\Gamma(1-\alpha)} \left[\frac{\phi^n}{\Delta t_{n+1}^\alpha} - \frac{\phi^0}{t_{n+1}^\alpha} - \alpha \sum_{i=1}^{K_{exp}} \omega_i U_{hist,i}^{n+1} \right], \tag{3.5} $$

where

$$U_{hist,i}^{n+1} = e^{-s_i\Delta t_{n+1}}U_{hist,i}^{n} + \frac{e^{-s_i\Delta t_{n+1}}}{s_i^2\Delta t_n}\Big[(e^{-s_i\Delta t_n} - 1 + s_i\Delta t_n)\phi^n + (1 - e^{-s_i\Delta t_n} - e^{-s_i\Delta t_n}s_i\Delta t_n)\phi^{n-1}\Big].$$

We further utilize the stabilized semi-implicit strategy to discretize the nonlinear terms to end up with linear schemes. Given the free energy E, we rewrite it as

$$E = \frac{1}{2}(\mathcal{L}\phi, \phi) + F, \tag{3.6}$$

where $\mathcal{L}$ is the linear operators that can be separated from E, and F is the rest of E, i.e., $F = E - \frac{1}{2}(\mathcal{L}\phi, \phi)$. With the notations above, the semi-discrete scheme for the fractional Allen–Cahn equation is given as follows.

Scheme 3.1 (Semi-Discrete Scheme for the Fractional Allen–Cahn Equation). Given ϕ^n, $n \geq 1$, we can get ϕ^{n+1} via

$${}_0^C D_t^\alpha \phi^{n+1} = -\lambda(\overline{\phi}^{n+1})\left(\mathcal{L}\phi^{n+1} - \overline{\frac{\delta F}{\delta \phi}}^{n+1}\right) + S_0\Delta(\phi^{n+1} - \overline{\phi}^{n+1}), \tag{3.7}$$

where $\overline{(\bullet)}^{n+1}$ is a second-order extrapolation, and S_0 is a stabilizing constant. The discrete operator ${}_0^C D_t^\alpha \phi^{n+1}$ is defined in (3.5).

The semi-discrete scheme for the fractional Cahn–Hilliard equation is given as follows.

Scheme 3.2 (Semi-Discrete Scheme for the Fractional Cahn–Hilliard Equation). Given ϕ^n, $n \geq 1$, we can get ϕ^{n+1} via

$${}_0^C D_t^\alpha \phi^{n+1} = \nabla\cdot\left(\lambda(\overline{\phi}^{n+1})\nabla(\mathcal{L}\phi^{n+1} + \overline{\frac{\delta F}{\delta \phi}}^{n+1})\right) - S_1\Delta^2(\phi^{n+1} - \overline{\phi}^{n+1}) + S_0\Delta(\phi^{n+1} - \overline{\phi}^{n+1}), \tag{3.8}$$

where $\overline{(\bullet)}^{n+1}$ is a second-order extrapolation, and S_0, S_1 are stabilizing constants. The discrete operator ${}_0^C D_t^\alpha \phi^{n+1}$ is defined in (3.5).

3.2. Compact finite difference spatial discretization

Here we further discretize the Scheme 3.1 and 3.2 in space using compact second order finite difference methods [14]. Consider a 2D domain $\Omega = [0, L_x] \times [0, L_y]$, where L_x and L_y are two positive real numbers. We divide the domain into rectangular meshes with uniform mesh sizes $h_x = L_x/N_x$, $h_y = L_y/N_y$, where N_x and N_y are the number of meshes in each direction.

Following the same notations as our previous work [14], we denote the sets E_x, E_y the edge-centered points for the uniform partition, and C_x, C_y the cell-centered points for the uniform partition, and functional spaces $\mathcal{C}_{x\times y}$ (center), $\mathcal{E}_{x\times y}^{ew}$ (east-west edges), and $\mathcal{E}_{x\times y}^{ns}$ (north-south edges). Define the center-to-east-west-edge average and difference operators $A_x, D_x : \mathcal{C}_{x\times y} \to \mathcal{E}_{x\times y}^{ew}$. and the center-to-north-south-edge average and difference operators $A_y, D_y : \mathcal{C}_{x\times y} \to \mathcal{E}_{x\times y}^{ns}$. Denote the full discrete Laplacian and biharmonic operator as

$$\Delta_h = d_x(D_x\phi) + d_y(D_y\phi), \quad \Delta_h^2 = \Delta_h(\Delta_h). \tag{3.9}$$

With the notations above, the full discrete, linear scheme for the fractional Allen–Cahn equation is given as follows.

Scheme 3.3 (Full Discrete Scheme for the Fractional Allen–Cahn Equation). Given ϕ^n, $n \geq 1$, we can get ϕ^{n+1} via

$${}_0^C D_t^\alpha \phi^{n+1} = \lambda\left[\mathcal{L}_h\phi^{n+1} - \overline{\left(\frac{\delta F}{\delta \phi}\right)}^{n+1}\right] + S_0\Delta_h(\phi^{n+1} - \overline{\phi}^{n+1}), \tag{3.10}$$

where $\overline{(\bullet)}^{n+1}$ is a second-order extrapolation, and S_0 is a stabilizing constant. The discrete operator ${}_0^C D_t^\alpha \phi^{n+1}$ is defined in (3.5).

The scheme for the fractional Cahn–Hilliard equation is given as follows.

Scheme 3.4 (Full Discrete Scheme for the Fractional Cahn–Hilliard Equation). Given ϕ^n, $n \geq 1$, we can get ϕ^{n+1} via

$$\begin{aligned}{}_0^C D_t^\alpha \phi^{n+1} = {} & d_x\cdot\left[A_x(\lambda(\overline{\phi}^{n+1}))D_x\left(\mathcal{L}_h\phi^{n+1}\right)\right] + d_y\cdot\left[A_y(\lambda(\overline{\phi}^{n+1}))D_y\left(\mathcal{L}_h\phi^{n+1}\right)\right] \\ & + d_x\cdot\left[A_x(\lambda(\overline{\phi}^{n+1}))D_x\left(\overline{\frac{\delta F}{\delta \phi}}^{n+1}\right)\right] + d_y\cdot\left[A_y(\lambda(\overline{\phi}^{n+1}))D_y\left(\overline{\frac{\delta F}{\delta \phi}}^{n+1}\right)\right] \\ & - S_1\Delta_h^2(\phi^{n+1} - \overline{\phi}^{n+1}) + S_0\Delta_h(\phi^{n+1} - \overline{\phi}^{n+1}),\end{aligned} \tag{3.11}$$

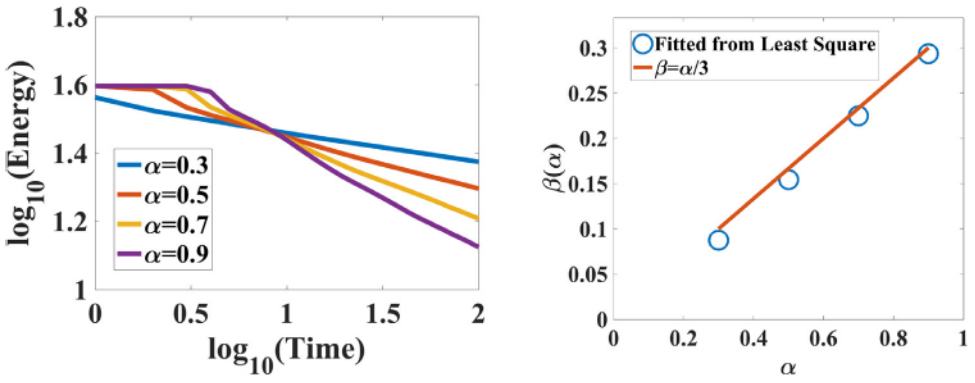

Fig. 4.1. Energy scaling laws for the FCH model with constant mobility $\lambda = \lambda_0$. (a) The log – log plot of the effective energy and time with different fractional-order α. (b) Energy decaying exponent $\beta(\alpha)$.

where $\overline{(\bullet)}^{n+1}$ is a second-order extrapolation, and S_0, S_1 are stabilizing constants. The discrete operator ${}_0^C D_t^\alpha \phi^{n+1}$ is defined in (3.5).

For detailed discussion on the choices of the stabilizing constants for Scheme 3.3 and 3.4, readers are referred to [24,37,44].

4. Power law scaling dynamics

In this section, we present our numerical findings on the time-fractional phase field models, that is the scaling of effective free energy/roughness in the time-fractional phase field models during coarsening follows a similar power law as the integer phase field models, where the power is linearly proportional to the fractional order α.

Here we consider a square domain $[0\ L]\times[0\ L]$ in 2D with L is the length in each direction, and choose periodic boundary conditions in the following discussion. Define the roughness measure function $W(t)$ as follows:

$$W(t) = \sqrt{\frac{1}{|\Omega|}\int_\Omega \Big(\phi(x,y,t) - \overline{\phi}(x,y,t)\Big)^2 d\Omega}, \tag{4.1}$$

where $\overline{\phi}(x,y,t) = \frac{1}{|\Omega|}\int_\Omega \phi(x,y,t)d\Omega$. It characterizes the fluctuations around its mean value. By the linear least square fitting, we get the absolute value of slope for each linear line of energy and roughness, $\beta(\alpha)$, $R(\alpha)$, defined as

$$\log_{10} E(\alpha,t) = \beta^0(\alpha) - \beta(\alpha)\log_{10} t, \quad \log_{10} W(\alpha,t) = R^0(\alpha) + R(\alpha)\log_{10} t. \tag{4.2}$$

where $E(\alpha, t)$ and $W(\alpha, t)$ are the energy function $E(t)$ and roughness function $W(t)$ with fractional order α respectively.

4.1. Power law scaling dynamics of the time fractional Cahn–Hilliard type equation

In the first example, we study the fractional Cahn–Hilliard (FCH) equation, equipped with the free energy

$$E = \int_\Omega \left[\frac{\varepsilon^2}{2}|\nabla\phi|^2 + \frac{1}{4}(1-\phi^2)^2\right] d\mathbf{x}, \tag{4.3}$$

where the first term represents the enthalpy, and the second term is the Ginsburg–Landau (double-well) bulk energy functional. The fractional Cahn–Hilliard equation with a variable mobility reads

$$\begin{cases} {}_0^C D_t^\alpha \phi = \nabla\cdot(\lambda(\phi)\nabla\mu), & (\mathbf{x},t)\in\Omega\times(0,T], \\ \mu = -\varepsilon^2\Delta\phi + \phi^3 - \phi, & (\mathbf{x},t)\in\Omega\times(0,T], \\ \phi(\mathbf{x},0) = \phi_0(\mathbf{x}), & \mathbf{x}\in\Omega, \end{cases} \tag{4.4}$$

where $\lambda(\phi)$ is the motility parameter, which could be chosen as [11]

$$(i)\lambda(\phi) = \lambda_0; \quad (ii)\lambda(\phi) = \lambda_0|1-\phi^2|; \quad (iii)\lambda(\phi) = \frac{\lambda_0}{2}|1+\phi|. \tag{4.5}$$

First of all, we conduct numerical study on the FCH Eq. (4.4) with a constant mobility $\lambda(\phi) = \lambda_0$. Follow the same setting as [11], i.e., consider a domain $[0,\ 4\pi]\times[0,\ 4\pi]$, and pick $\varepsilon = 0.05$, $\lambda_0 = 0.02$, and choose random initial condition $\phi|_{t=0} = 0.001\times rand(-1,1)$. The results are summarized in Fig. 4.1, where we have simulated several situations with

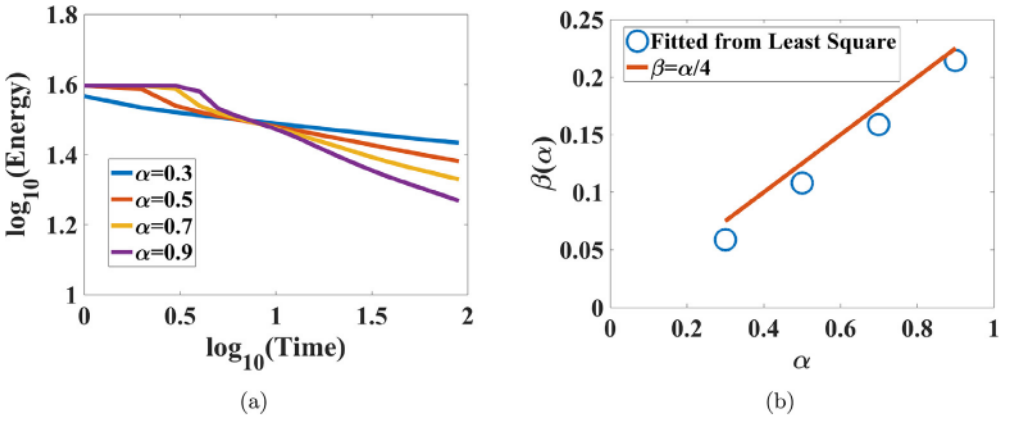

Fig. 4.2. Energy scaling laws for the FCH model with variable mobility $\lambda = \lambda_0|1-\phi^2|$. (a) The log − log plot of the effective energy and time with different fractional-order α. (b) Energy decaying exponent $\beta(\alpha)$. This figure illustrates that the effective energy decays as $O(t^{-\frac{\alpha}{4}})$, which is consistent with $O(t^{-\frac{1}{4}})$ as indicated in [11] for the integer Cahn–Hilliard equation.

$\alpha = 0.3, 0.5, 0.7$ and 0.9. We observe the energy scales approximately as $O(t^{-\frac{\alpha}{3}})$, which is consistent with $O(t^{-\frac{1}{3}})$ as indicated in [11] for the integer Cahn–Hilliard equation with constant mobility, i.e. the power of the power-law scaling is linearly proportional to the fractional order α.

Next, we study the FCH Eq. (4.4) with variable mobility $\lambda(\phi) = \lambda_0|1-\phi^2|$. We use the same initial values and parameters as the example above. The energy plot at different time slots with various fractional orders are summarized in Fig. 4.2. We observe that the energy scales approximately like $O(t^{-\frac{\alpha}{4}})$, which is consistent with $O(t^{-\frac{1}{4}})$ as indicated in [11] for the integer Cahn–Hilliard equation with variable mobility $\lambda(\phi) = \lambda_0|1-\phi^2|$.

To better understand the dynamics induced by the time-fractional phase field models, we present a time series of 2D snapshots for the coarsening dynamics. We point out that the difference between the time-fractional phase field models and integer phase field models lie in the timescales of coarsening. After rescaling, models with different fractional order α predict qualitative similar patterns.

Remark 4.1. Rigorous analysis and comparisons on pattern formation between the CH and FCH models would be out of this paper's scope. Here we point out several nice references for interested readers. A good review on the integer phase field model formulation, numerical approximations and different instability mechanisms could be found in [18]. Experiment calibrations on the Cahn–Hilliard equation with stability analysis is available in [15]. Some seminal work on discovering how the order of the fractional derivative can change conditions of instability and longtime dynamics in time-fractional partial differential equations include [4,12,42].

First of all, some 2D snapshots at different time slots are presented in Fig. 4.3 for the FCH model (4.4) with constant mobility $\lambda = \lambda_0$. As indicated in Fig. 4.1, the FCH model with larger fractional order α has faster evolution dynamics, which is consistent with the observation in Fig. 4.3. But the patterns resulted from the FCH model with different fractional order α are qualitatively similar, saying if we compare Fig. 4.3 (b)-5, (c)-3 and (d)-2. In other words, tuning the fractional order is a good mechanism for tuning the timescales, which could be utilized to model anomalous dynamics for mixtures with memory effects or long-range interactions.

The corresponding coarsening dynamics for FCH model (4.4) with variable mobility $\lambda(\phi) = \lambda_0|1-\phi^2|$ at different time steps are summarized in Fig. 4.4. We observe that FCH models with different fractional order α predict qualitative similar coarsening patterns, and it is the time scale that differs from each other. Mainly larger fractional order leads to faster evolution dynamics, which is consistent with the energy decaying dynamics in Fig. 4.2.

4.2. Power law scaling dynamics of the time-fractional Allen–Cahn type equation

In the second example, we study the time fractional Allen–Cahn type equation. In particular, we consider fractional molecular beam epitaxy (FMBE) model. Given a smooth domain Ω, we use $\phi(\mathbf{x}, t) : \Omega \to \mathbb{R}$ to denote the height function of MBE. The effective free energy is proposed as

$$E(\phi) = \int_\Omega \left[\frac{\varepsilon^2}{2}|\Delta\phi|^2 + f(\nabla\phi)\right] d\Omega. \tag{4.6}$$

Here the first term represents the isotropic surface diffusion effect with ε a constant controlling the surface diffusion strength, and the second term approximates the Enrlich–Schwoebel effect that the adatoms stick to the boundary from an upper terrace, contributing to the steepening of mounds in the film [10].

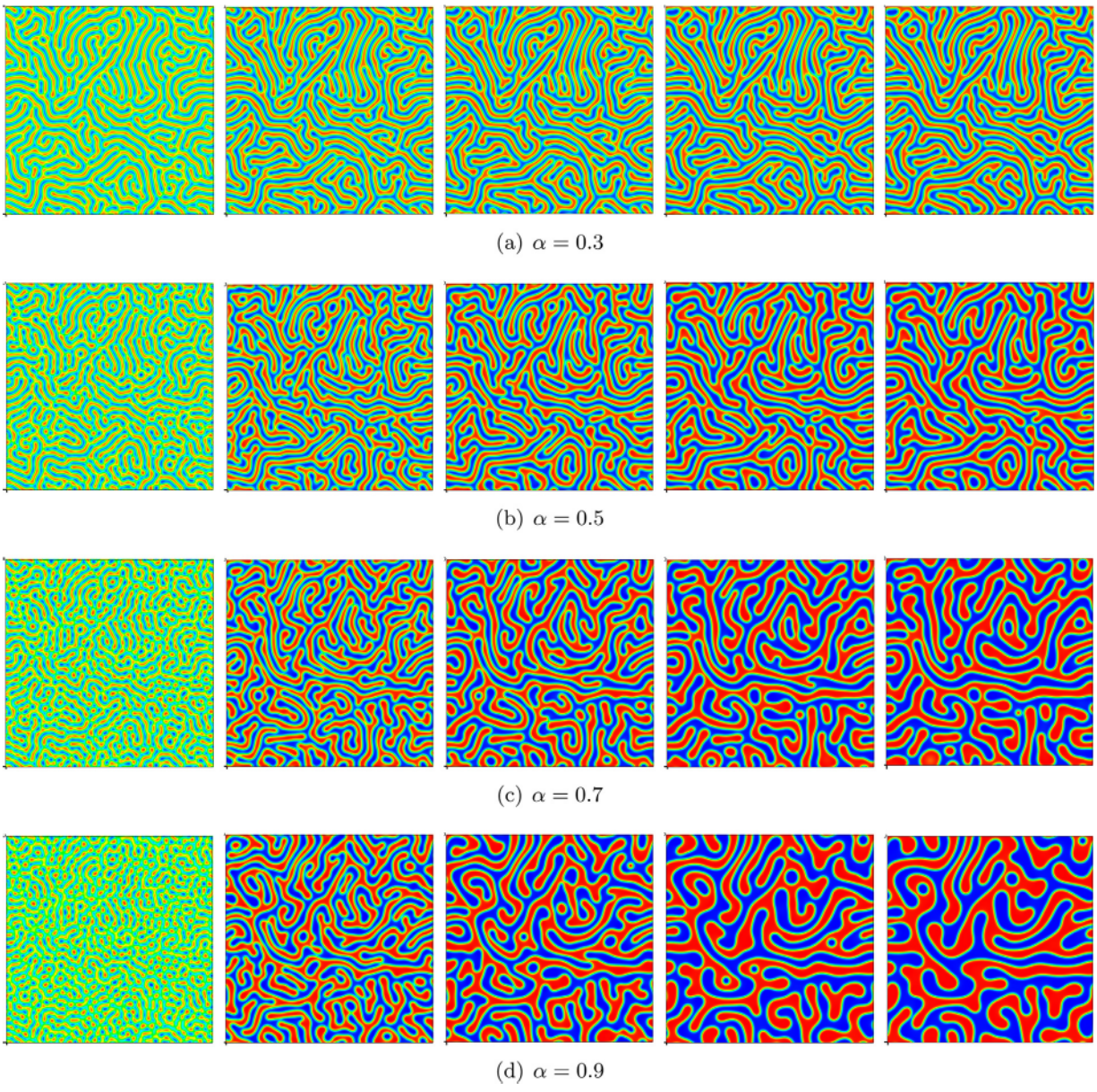

Fig. 4.3. Time snapshots of coarsening dynamics driven by the FCH model (2.9) with constant mobility $\lambda = \lambda_0$. (a–d) The profiles of ϕ at $t = 5, 25, 50, 100, 150$ for various fractional order $\alpha = 0.3, 0.5, 0.7$ and 0.9 are presented, respectively.

If we choose $f(\nabla\phi) = \frac{1}{4}(|\nabla\phi|^2 - 1)^2$, the corresponding FMBE model with slope selection reads

$$\begin{cases} {}_0^C D_t^\alpha \phi(\mathbf{x}, t) = -M\Big(\varepsilon^2 \Delta^2 \phi - \nabla \cdot ((|\nabla\phi|^2 - 1)\nabla\phi)\Big), \ (\mathbf{x}, t) \in \Omega \times (0, T], \\ \phi(\mathbf{x}, 0) = \phi_0(\mathbf{x}), \quad \mathbf{x} \in \Omega. \end{cases} \tag{4.7}$$

For the FMBE model with slope selection, the energy scaling laws are summarized in Fig. 4.5. It indicates that the energy scales approximately like $O(t^{-\frac{\alpha}{3}})$, which is consistent with $O(t^{-\frac{1}{3}})$ as indicated in [43] for the integer MBE equation with slope selection. Similarly, as shown in Fig. 4.6, the roughness scales approximately like $O(t^{\frac{\alpha}{3}})$, which is consistent with $O(t^{\frac{1}{3}})$ as indicated in [43] for the integer MBE equation with slope selection.

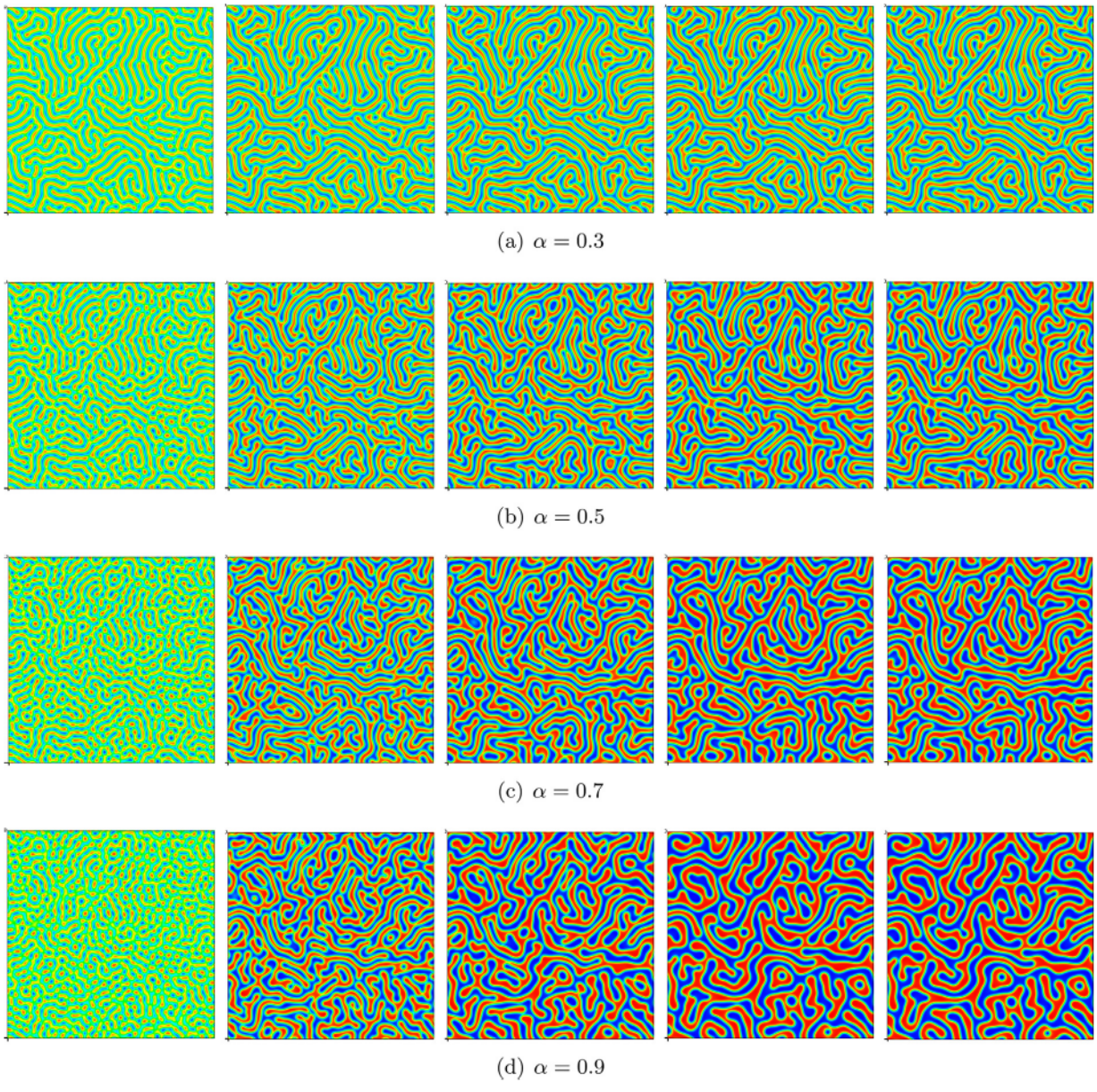

Fig. 4.4. Time snapshots of coarsening dynamics driven by the FCH model with variable mobility $\lambda = \lambda_0|1-\phi^2|$. (a–d) The profiles of ϕ at $t = 5, 25, 50, 100, 125$ for various fractional order $\alpha = 0.3, 0.5, 0.7$ and 0.9 are presented, respectively.

On the other hand, if we choose $f(\nabla\phi) = -\frac{1}{2}\ln(1+|\nabla\phi|^2)$, the corresponding time-fractional MBE model without slope selection reads

$$\begin{cases} {}_0^C D_t^\alpha \phi(\mathbf{x},t) = -M\Big(\varepsilon^2\Delta^2\phi + \nabla\cdot\big(\dfrac{\nabla\phi}{1+|\nabla\phi|^2}\big)\Big), \ (\mathbf{x},t)\in\Omega\times(0,T], \\ \phi(\mathbf{x},0) = \phi_0(\mathbf{x}), \quad \mathbf{x}\in\Omega. \end{cases} \tag{4.8}$$

For the time-fractional MBE model without slope selection, the roughness scales approximately like $O(t^{\frac{\alpha}{2}})$, which is consistent with $O(t^{\frac{1}{2}})$ as indicated in [43] for the integer MBE equation without slope selection. The results are summarized in Fig. 4.7.

Time sequences of roughness ($\Delta\phi$) for the time-fractional MBE models are summarized in Fig. 4.8 (with slope selection) and Fig. 4.9 (without slope selection). They predict qualitative similar patterns as the integer MBE models [9,23,43,47]. And we also observer the time-fractional MBE models with larger fractional order α evolve faster, which agrees with the energy/roughness scaling as presented in Fig. 4.5 and Fig. 4.6.

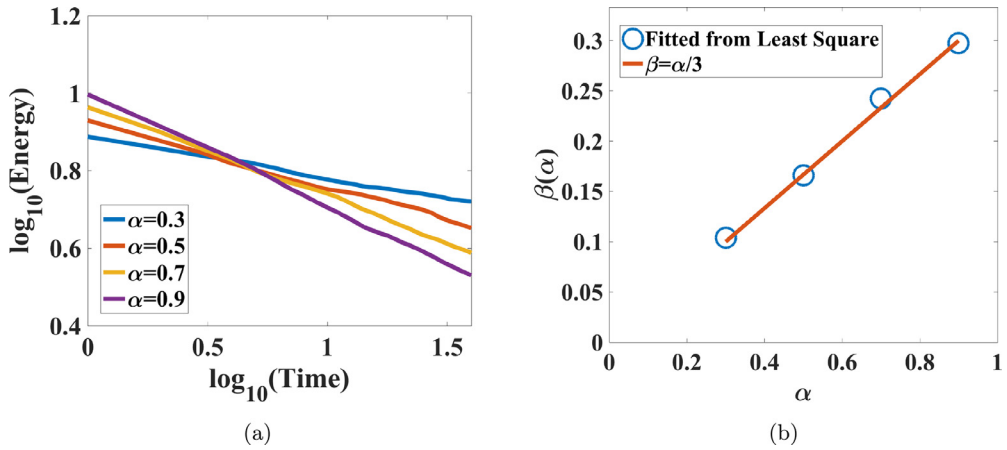

Fig. 4.5. Energy scaling laws for the time-fractional molecular beam epitaxy equation with slope selection. (a) The log – log plot of the effective energy and time with different fractional-order α. (b) The least-square fitted energy decay power β for different fractional order α.

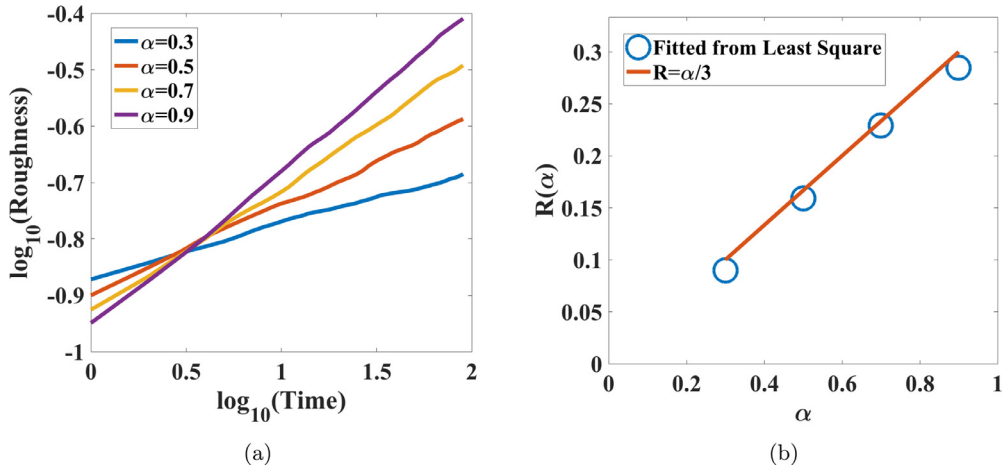

Fig. 4.6. Roughness scaling laws for the FMBE model with slope selection. (a) The log – log plot of the roughness and time with different fractional-order α. (b) The least-square fitted roughness growth power $R(\alpha)$ for different fractional order α.

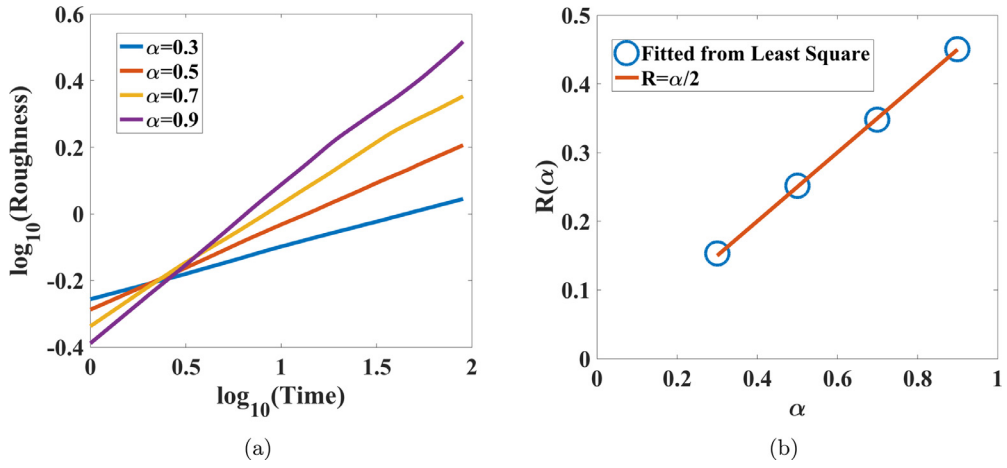

Fig. 4.7. Roughness growth scaling laws for the FMBE model without slope selection. (a) The log – log plot of the roughness and time with different fractional-order α. (b) The least-square fitted roughness growth power $R(\alpha)$ for different fractional order α.

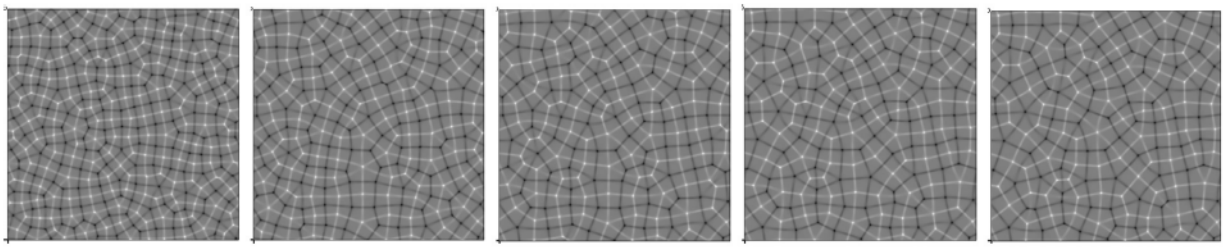

(a) $\alpha = 0.3$

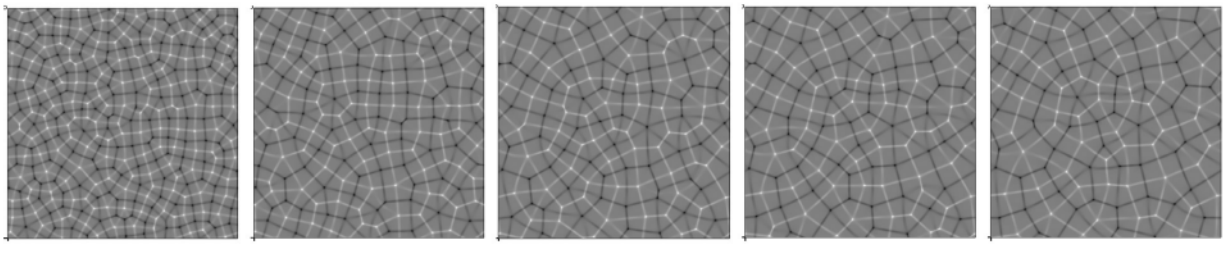

(b) $\alpha = 0.5$

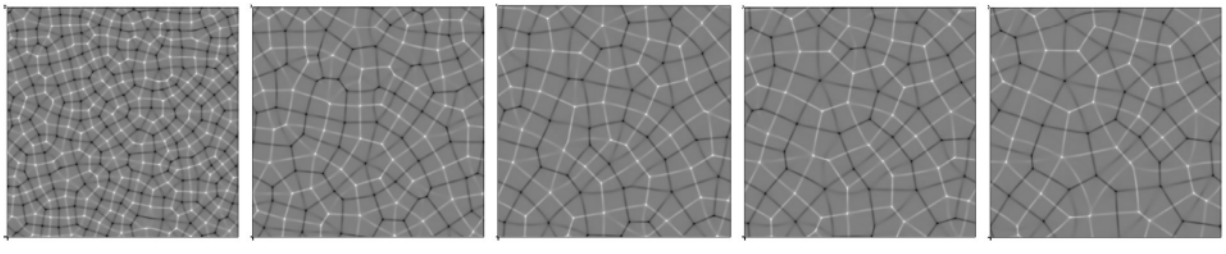

(c) $\alpha = 0.7$

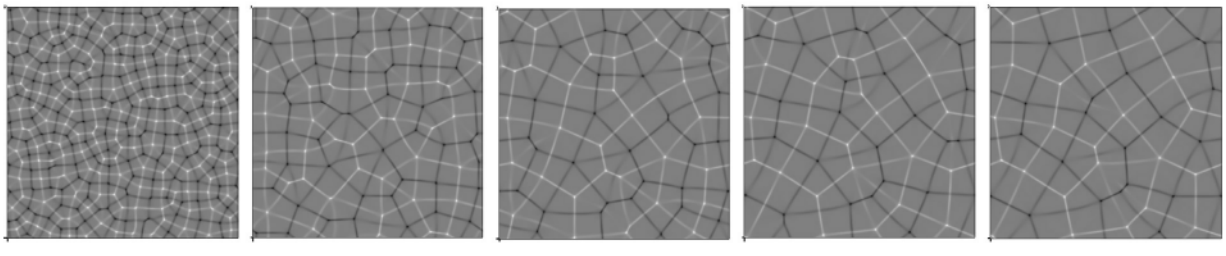

(d) $\alpha = 0.9$

Fig. 4.8. Time snapshots of the roughness ($\Delta\phi$) evolution of the FMBE model with slope selection. (a-d) The snapshots of $\Delta\phi$ at time $t =$ 5, 50, 100, 150, 200 for various fractional order $\alpha = 0.3$, 0.5, 0.7 and 0.9 are presented, respectively.

5. Conclusion

In this paper, we focus on the time-fractional phase field models (the Allen–Cahn equation and the Cahn–Hilliard equation) and their scaling laws during coarsening dynamics, discovering correlations of effective energy scaling laws and the fractional order α.

For the time-fractional Cahn–Hilliard equation, we study the power law scaling behavior of effective free energies with both constant mobility and variable mobility in coarsening dynamics. For FCH model with constant mobility, the effective free energy scales as $O(t^{-\frac{\alpha}{3}})$, which is consistent with the well known result $(t^{-\frac{1}{3}})$ for integer order Cahn–Hilliard model [11]. For the FCH model with phase-variable dependent mobility $\lambda = \lambda_0|1-\phi^2|$, the effective free energy scales as $O(t^{-\frac{\alpha}{4}})$, which is consistent with the result of $O(t^{-\frac{1}{4}})$ for the integer Cahn–Hilliard equation with such variable mobility.

For the time-fractional molecular beam epitaxy (MBE) model, the scaling behavior of the effective free energies and roughnesses has been investigated. Specifically, we observe: the effective free energy decays as $O(t^{-\frac{\alpha}{3}})$ and the roughness grows as $O(t^{\frac{\alpha}{3}})$ for the MBE model with slope selection; and the roughness grows as $O(t^{\frac{\alpha}{2}})$ for the MBE model without

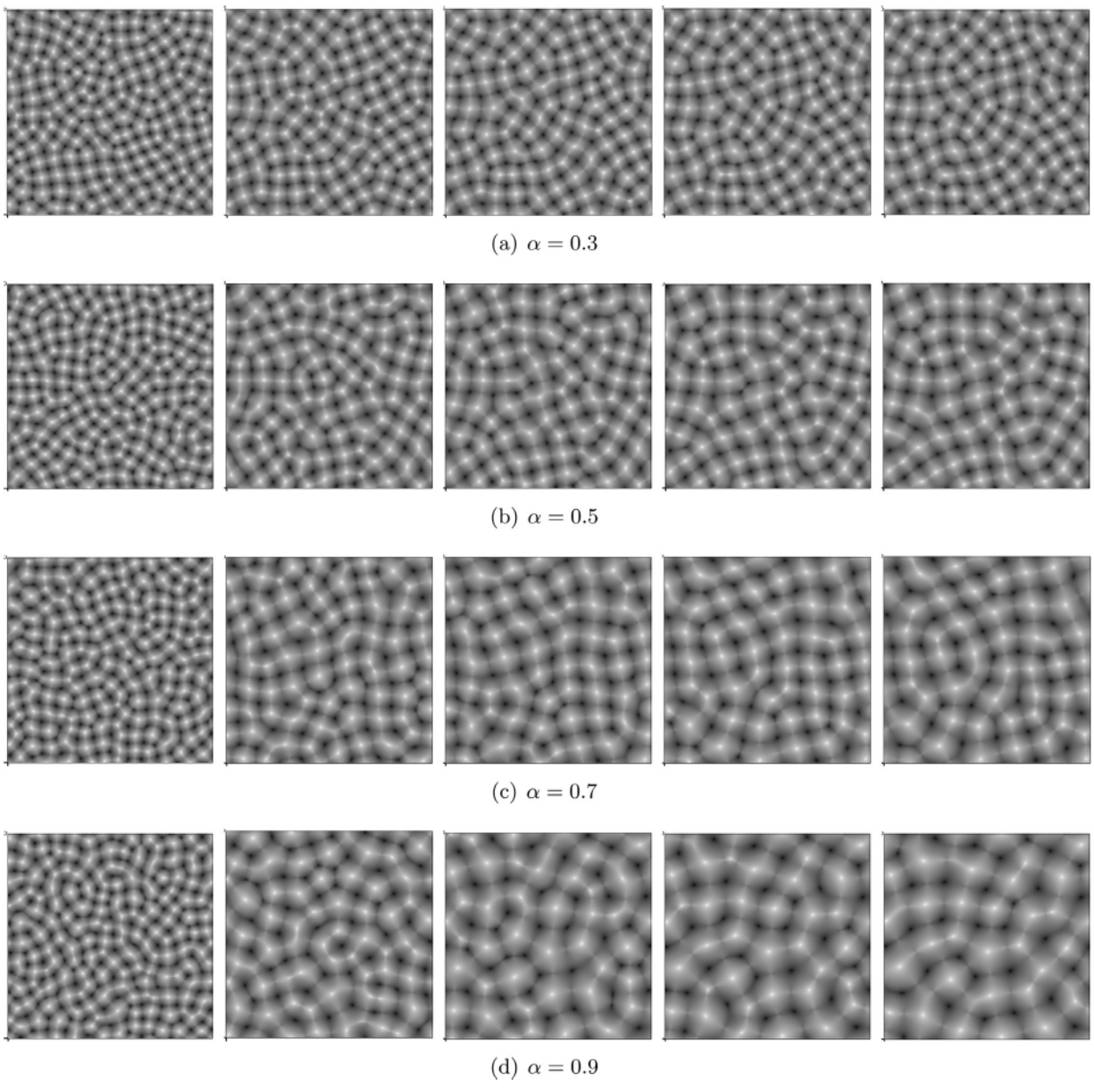

Fig. 4.9. Time snapshots of the roughness ($\Delta\phi$) evolution of FMBE model without slope selection. (a-d) The snapshots of $\Delta\phi$ at time $t = 5, 50, 100, 150, 200$ for fractional order $\alpha = 0.3, 0.5, 0.7$ and 0.9 are presented, respectively.

slope selection. That is to say, the coarsening rate of MBE model could be manipulated by the fractional order α, and it follows a power law with the power linearly proportional to α.

Overall, we investigate time-fractional phase field models and discover a general power-law scaling property. *The effective free energy/roughness of the time-fractional phase field models during coarsening follows a similar power scaling law as the integer phase field models, where the power is linearly proportional to the fractional order* α. These general power-law scaling dynamics are verified numerically against several phase field models, including the Cahn–Hilliard (CH) equations with different variable mobilities and molecular beam epitaxy (MBE) models. This is the first time in literature to report/discover such scaling correlation. This new finding sheds light on applying time-fractional phase field models in studying anomalous coarsening dynamics. Rigorous asymptotic analysis of this interesting correlation will be pursed in our future work.

Acknowledgment

Jia Zhao is partially supported by the National Science Foundation under Grant DMS-1816783, and a seed grant (Research Catalyst Grant) from the Office of Research and Graduate Studies at Utah State University. Lizhen Chen would like to

acknowledge the support from National Science Foundation of China through Grant 11671166 and U1530401, Postdoctoral Science Foundation of China through Grant 2015M580038. Hong Wang is partially supported by the OSD/ARO MURI Grant W911NF-15-1-0562 and by the National Science Foundation under Grant DMS-1620194.

References

[1] Alikhanov A. A new difference scheme for the time fractional diffusion equation. J Comput Phys 2015;280:424–38.
[2] Allen SM, Cahn JW. A microscopic theory for antiphase boundary motion and its application to antiphase domain coarsening. Acta Metall Mater 1979;27:1085–95.
[3] Anderson DM, Mcfadden GB, Wheeler AA. Diffuse-interface methods in fluid mechanics. Annu Rev Fluid Mech 1998;30(1):139–65.
[4] Gafiychuk V, Datsko B, Luchko Y. Pattern formation in fractional reaction–diffusion systems with multiple homogeneous states. J Bifurc Chaos 2012;22(4):1250087.
[5] Benson D, Schumer R, Meerschaert MM, Wheatcraft SW. Fractional dispersion, Levy motions, and the MADE tracer tests. Transp Porous Media 2001;42:211–40.
[6] Brannick J, Liu C, Qian T, Sun H. Diffuse interface methods for multiple phase materials: an energetic variational approach. Numer Math Theory Methods Appl 2015;8:220–36.
[7] Cahn JW. Free energy of a nonuniform system. ii. thermodynamic basis. J Chem Phys 1959;30(5):1121–4.
[8] Cahn JW, Hilliard JE. Free energy of a nonuniform system. i. interfacial free energy. J Chem Phys 1958;28:258–67.
[9] Chen L., Zhao J., Cao W., Wang H., Zhang J.. An accurate and efficient algorithm for the time-fractional molecular beam epitaxy model with slope selection. arXiv:1803.01963, (submitted for publication).
[10] Chen W, Wang C, Wang X, Wise SM. A linear iteration algorithm for a second-order energy stable scheme for a thin film model without slope selection. J Sci Comput 2014;59(3):574–601.
[11] Dai S, Du Q. Computational studies of coarsening rates for the Cahn–Hilliard equation with phase-dependent diffusion mobility. J Comput Phys 2016;310:85–108.
[12] Gafiychuk V, Datsko B. Mathematical modeling of different types of instabilities in time fractional reaction–diffusion systems. Comput Math Appl 2010;59(3):1101–7.
[13] Golubovic L. Interfacial coarsening in epitaxial growth models without slope selection. Phys Rev Lett 1997;78:90–3.
[14] Gong Y, Zhao J, Wang Q, Sci J. Second order fully discrete energy stable methods on staggered grids for hydrodynamic phase field models of binary viscous fluids. SIAM Comput 2018;40(2):B528–53.
[15] Hulikalz S, Chen C, Chasona E, Bower A. Experimental calibration of a Cahn–Hilliard phase-field model for phase transformations in Li-Sn electrodes. J Electrochem Soc 2016;163(13):A2647–59.
[16] Jiang S, Zhang J, Zhang Q, Zhang ZM. Fast evaluation of the Caputo fractional derivative and its applications to fractional diffusion equations. Commun Comput Phys 2017;21(3):650–78.
[17] Kapustina M, Tsygankov D, Zhao J, Wesller T, Yang X, Chen A, Roach N, Elston TC, Wang Q, Jacobson K, Forest MG. Modeling the excess cell membrane stored in a complex morphology of bleb-like protrusions. PLoS Comput Biol 2016;12(3):e1004841.
[18] Kim J. Phase-field models for multi-component fluid flows. Commun Comput Phys 2012;12(3):613–61.
[19] Kohn R, Otto F. Upper bounds on coarsening rates. Commun Math Phys 2002;229:375–95.
[20] Kohn RV, Yan X. Upper bound on the coarsening rate for an epitaxial growth model. Comm Pure Appl Math 2003;56:1549–64.
[21] Langlands TAM, Henry BI, Wearne SL. Fractional cable equation models for anomalous electrodiffusion in nerve cells: infinite domain solutions. J Math Biol 2009;59:761–808.
[22] Li B, Liu J. Epitaxial growth without slope selection: energetics, coarsening and dynamic scaling. J Nonlinear Sci 2004;14:429–51.
[23] Li B, Liu JG. Thin film epitaxy with or without slope selection. Eur J Appl Math 2003;14:713–43.
[24] Li D, Qiao Z, Tang T. Characterizing the stabilization size for semi-implicit Fourier-spectral method to phase field equations. SIAM J Numer Anal 2016;54(3):1653–81.
[25] Li X, Xu C. A space-time spectral method for the time fractional diffusion equation. SIAM J Numer Anal 2009;47(3):2108–31.
[26] Li Y, Kim J. Phase field simulations of crystal growth with adaptive mesh refinement. Int J Heat Mass Transf 2012;55:7926–32.
[27] Li Z, Wang H, Yang D. A space-time fractional phase-field model with tunable sharpness and decay behavior and its efficient numerical simulation. J Comput Phys 2017;347:20–38.
[28] Lin Y, Xu C. Finite difference spectral approximations for the time-fractional diffusion equation. J Comput Phys 2007;225:1533–52.
[29] Mata M, Garcia-Cervera C, Ceniceros H. Ordering kinetics of a conserved binary mixture with a nematic liquid crystal component. J Non Newton Fluid Mech 2014;212:18–27.
[30] Metzler R, Klafter J. The random walk's guide to anomalous diffusion: a fractional dynamics approach. Phys Rep 2000;339:1–77.
[31] Metzler R, Klafter J. The restaurant at the end of the random walk: recent developments in the description of anomalous transport by fractional dynamics. J Phys A Math Gen 2004;37:R161–208.
[32] Min W, Luo G, Cheayil BJ, Kou SC, Xie XS. Observation of a power-law memory kernel for fluctuations within a single protein molecule. Phys Rev Lett 2005;94:198302.
[33] Najem S, Grant M. Phase-field model for collective cell migration. Phys Rev E 2016;93(052405).
[34] Podlubny I. Fractional Differential Equations. Academic Press; 1999.
[35] Ramos-Fernandez G, Mateos J, Miramontes O, Cocho G, Larralde H, Ayala-Orozco B. Levywalk patterns in the foraging movements of spider monkeys (Ateles geoffroyi). Behav Ecol Sociobiol 2004;55:223–30.
[36] Shao D, Pappel W, Levine H. Computational model for cell morphodynamics. Phys Rev Lett 2010;105.
[37] Shen J, Yang X. Numerical approximations of Allen–Cahn and Cahn–Hilliard equations. Discret Contin Dyn Syst A 2010;28:1669–91.
[38] Shen J, Yang X. Decoupled energy stable schems for phase field models of two phase complex fluids. SIAM J Sci Comput 2014;36(1):122–45.
[39] Song F, Xu C, Karniadakis G. A fractional phase-field model for two-phase flows with tunable sharpness: algorithms and simulations. Comput Methods Appl Mech Eng 2016;305:376–404.
[40] Tanaka S, Kubo Y, Yokoyama Y, Toda A, Taguchi K, Kajioka H. Kinetics of phase separation and coarsening in dilute surfactant pentaethylene glycol monododecyl ether solution. J Chem Phys 2011;135:234503.
[41] Taniguchi T, Onuki A. Network domain structure in viscoelastic phase separation. Phys Rev Lett 1996;77(24):4910–13.
[42] Datsko B, Gafiychuk V. Different types of instabilities and complex dynamics in reaction–diffusion systems with fractional derivatives. J Comput Nonlinear Dyn 2012;7(3):031001.
[43] Wang C, Wang X, Wise S. Unconditionally stable schemes for equations of thin film epitaxy. Discret Contin Dyn Syst 2010;28(1):405–23.
[44] Wang L, Yu H. On Efficient second order stabilized semi-implicit schemes for the Cahn-Hilliard phase-field equaiton. J Sci Comput 2018;77(2):1185–209.
[45] Wise S, Lowengrub J, Frieboes H, Cristini B. Three dimensional multispecies nonlinear tumor growth i: model and numerical method. J Theor Biol 2008;253(3):524–43.
[46] Yan Y, Sun Z, Zhang J. Fast evaluation of the Caputo fractional derivative and its applications to fractional diffusion equations: a second-order scheme. Commun Comput Phys 2017;22(4):1028–48.
[47] Yang X, Zhao J, Wang Q. Numerical approximations for the molecular beam epitaxial growth model based on the invariant energy quadratization method. J Comput Phys 2017;333:102–27.

[48] Yang X, Zhao J, Wang Q, Shen J. Numerical approximations for a three components Cahn–Hilliard phase-field model based on the invariant energy quadratization method. Math Models Methods Appl Sci 2017;27:1993–2023.
[49] Yue P, Feng JJ, Liu C, Shen J. Diffuse interface simulations of drop coalescence and retraction in viscoelastic fluids. J Non Newton Fluid Mech 2005;129:163–76.
[50] Zhao J, Shen Y, Happasalo M, Wang ZJ, Wang Q. A 3d numerical study of antimicrobial persistence in heterogeneous multi-species biofilms. J Theor Biol 2016;392:83–98.
[51] Zhao J, Wang Q, Yang X. Numerical approximations for a phase field dendritic crystal growth model based on invariant energy quadratization. Int J Numer Methods Eng 2017;110(3):279–300.
[52] Zhu J, Chen L, Shen J, Tikare V. Coarsening kinetics from a variable-mobility Cahn–Hilliard equation: application of a semi-implicit Fourier spectral method. Phys Rev E 1999;60(4):3564–72.
[53] Ziebert F, Aranson IS. Effects of adhesion dynamics and substrate compliance on the shape and motility of crawling cells. PLOS ONE 2013;8(5):e64511.